

Pauli Noise Learning for Mid-Circuit Measurements

Jordan Hines^{1,2,*} and Timothy Proctor^{2,†}

¹Department of Physics, University of California, Berkeley, CA 94720

²Quantum Performance Laboratory, Sandia National Laboratories, Livermore, CA 94550

Current benchmarks for mid-circuit measurements (MCMs) are limited in scalability or the types of error they can quantify, necessitating new techniques for quantifying their performance. Here, we introduce a theory for learning Pauli noise in MCMs and use it to create MCM cycle benchmarking, a scalable method for benchmarking MCMs. MCM cycle benchmarking extracts detailed information about the rates of errors in randomly compiled layers of MCMs and Clifford gates, and we demonstrate how its results can be used to quantify correlated errors during MCMs on current quantum hardware. Our method can be integrated into existing Pauli noise learning techniques to scalably characterize and benchmark wide classes of circuits containing MCMs.

Mid-circuit measurements (MCMs) are a critical component of quantum error correction [1–5] and some quantum algorithms [6–8], but they are often a large source of error in contemporary quantum processors [2–5, 9–12]. Despite this, there are currently few techniques capable of quantifying the errors in MCMs, and those that can are limited in scope or scalability. Full tomography of MCMs [9, 10] is computationally expensive and only feasible for small systems, whereas more scalable methods based on randomized benchmarking (RB) [11, 12] are restricted to assessing crosstalk errors caused by MCMs and provide limited quantitative information.

Pauli noise learning [13–17] is a family of methods for characterizing ideally unitary gates that offers an intermediate approach of partial characterization, between the extremes of fully tomography and RB. These techniques are widely used, they enable error mitigation [18–20], and they can characterize some of the errors in syndrome extraction circuits [21, 22]. However, because noise in MCMs cannot be tailored into the same stochastic Pauli error structure as gate error [23, 24], existing Pauli noise learning techniques cannot fully characterize MCMs, and this limits their application to measurement noise [20, 25].

In this letter, we introduce and demonstrate Pauli noise learning techniques for MCMs. We introduce theory for Pauli noise learning of uniform stochastic instruments (USIs) [26], a stochastic noise model for circuit layers (i.e., cycles) containing MCMs that can be enforced using a recent extension of randomized compilation [23] to MCM-containing layers [27]. We apply this theory to introduce MCM cycle benchmarking (MCM-CB), which is a scalable protocol for estimating the fidelity of MCM-containing layers (a.k.a. cycles) that generalizes the cycle benchmarking protocol [28, 29]. We then show how to jointly characterize multi-qubit Clifford gates and MCMs, learning parameters of the MCM and gate error that cannot be learned by characterizing the individual components in isolation.

Mid-circuit measurements—First we define some notation. We use \mathbb{P}_n to denote the n -qubit Pauli operators (without

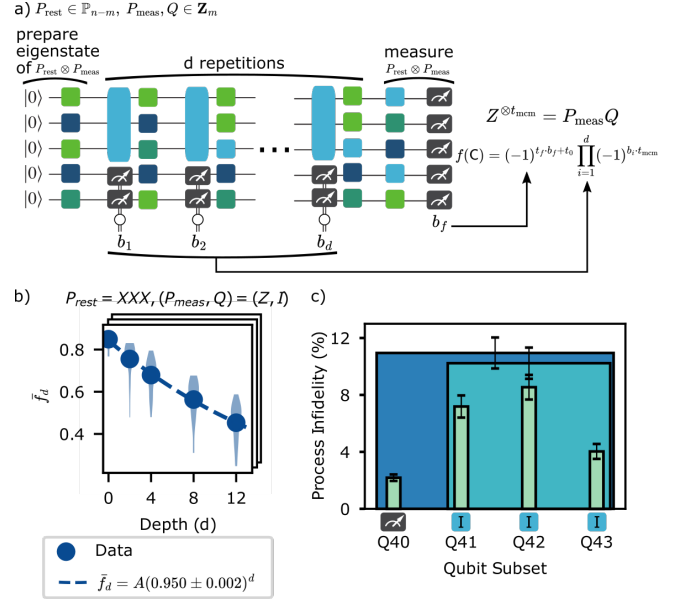


FIGURE 1. Estimating the fidelity of MCM layers with MCM-CB. Our protocol consists of running a random selection of subexperiments parameterized by Pauli operators P_{rest} , P_{meas} , and Q . (a) Each subexperiment runs circuits with d repetitions of a randomly compiled layer \bar{L} and measures $P_{\text{rest}} \otimes P_{\text{meas}}$. This measurement result is then modified by the MCM results using an analysis determined by $P_{\text{meas}} Q$ to compute a figure-of-merit $f(C)$, which is averaged over circuits of depth d to obtain \bar{f}_d . (b) Each subexperiment's \bar{f}_d is fit to an exponential, and the fit decay constants from many subexperiments are used to estimate the fidelity of \bar{L} . (c) Infidelity estimates from MCM-CB on `ibm_osaka` for a layer consisting of one MCM (on Q40) and 3 idling qubits (Q41–Q43). Error on the idling qubits is dominant, and the high infidelity of the individual qubits is indicative of correlated error.

signs). For $a \in \mathbb{Z}_2^k$, we use $P^{\otimes a}$ to denote the Pauli operator $P^{a_1} \otimes P^{a_2} \otimes \dots \otimes P^{a_k}$, and we call Pauli operators with this form P -type Pauli operators. We use \mathcal{P} to denote the superoperator representation of P . We denote the set of m -qubit Z -type Pauli operators by \mathbf{Z}_m .

An n -qubit *MCM layer* L is a set of instructions to perform projective measurements on m qubits and unitary gates on the remaining $n - m$ qubits. We will consider MCM layers containing only computational basis measurements (extension to

* jordanh@berkeley.edu

† tjproct@sandia.gov

other Pauli bases is simple), and Clifford gates. If run without error, a quantum processor implementing L performs the process

$$\mathcal{L} = \sum_{k \in \mathbb{Z}_2^m} \mathcal{V} \otimes |k\rangle\langle k| \otimes |k\rangle, \quad (1)$$

where $|k\rangle$ denotes the classical outcome of the MCM, $|k\rangle \equiv ||k\rangle\langle k|$, and $|\rho\rangle\rangle$ is the vector representing operator ρ in Hilbert-Schmidt space $[\mathcal{B}(\mathcal{H})]$, and \mathcal{V} is the superoperator representation of the unitary acting on the unmeasured qubits.

An imperfect implementation of L can be represented as a quantum instrument $\mathcal{M} : \mathcal{B}(\mathcal{H}) \rightarrow \mathcal{B}(\mathcal{H}) \otimes \mathbb{Z}_2^m$ of the form

$$\mathcal{M} = \sum_{k \in \mathbb{Z}_2^m} \mathcal{M}_k \otimes |k\rangle, \quad (2)$$

where each \mathcal{M}_k is completely positive and trace non-increasing and $\sum_{k \in \mathbb{Z}_2^m} \mathcal{M}_k$ is trace preserving [9, 10]. The process (i.e., entanglement) fidelity of \mathcal{M} to \mathcal{L} satisfies [26]

$$F(\mathcal{M}) \equiv F(\mathcal{M}, \mathcal{L}) = \left(\sum_{k \in \mathbb{Z}_2^m} \sqrt{F(\mathcal{M}_k, \mathcal{V} \otimes |k\rangle\langle k|)} \right)^2. \quad (3)$$

Uniform stochastic instruments—Our method is designed to learn the error of *uniform stochastic instruments* (USIs), a class of quantum instruments with a simple form of stochastic Pauli error. USIs have the form

$$\overline{\mathcal{M}} = \sum_{k \in \mathbb{Z}_2^m} \overline{\mathcal{M}}_k \otimes |k\rangle, \quad (4)$$

where

$$\overline{\mathcal{M}}_k = \sum_{a, b \in \mathbb{Z}_2^m} \mathcal{T}_{a, b} \mathcal{V} \otimes \mathcal{X}^{\otimes b} |k\rangle\langle k| \mathcal{X}^{\otimes a}. \quad (5)$$

The $\mathcal{T}_{a, b}$ are unnormalized $(n - m)$ -qubit stochastic Pauli channels acting on the unmeasured qubits, and they satisfy $\sum_{a, b \in \mathbb{Z}_2^m} \text{Tr}(\mathcal{T}_{a, b}) = 1$ [24]. The probability that the pre-measurement error \mathcal{X}^a and the post-measurement error \mathcal{X}^b occur is $\text{Tr}(\mathcal{T}_{a, b})$. The process fidelity of $\overline{\mathcal{M}}$ is $F(\overline{\mathcal{M}}) = \text{Tr}(\mathcal{T}_{0, 0})$, which is the probability of no error [26].

Our method uses *randomized compiling* for MCM layers [23, 24] to enforce a USI model for all MCM layers. The randomized compilation of an MCM layer L is a composite layer $\overline{L} = T_0 L T_0'$ (read left to right), where T_0 consists of uniformly random Pauli gates applied to each qubit and T_0' is the inverse of T_0 , composed with a uniformly random layer of Z gates. For each measured qubit in L , if T_0 contains an X or Y gate on that qubit, its classical MCM outcome is flipped. In a circuit with multiple layers, adjacent layers of Pauli gates are typically compiled together. Whenever the single-qubit gate error is small relative to the error in \mathcal{M} , which we assume hereafter, an imperfect implementation of \overline{L} is approximately a USI.

Theory of learning USIs—We now introduce our theory for learning USIs. For now we assume that the unmeasured subsystem's error-free evolution is $\mathcal{V} = \mathbb{I}_{n-m}$, and we consider

the more general case in the SM. To completely determine a USI [Eq. (4)], we must learn the stochastic Pauli channels $\mathcal{T}_{a, b}$ for all $a, b \in \mathbb{Z}_2^m$. Stochastic Pauli channels are diagonal in the Pauli transfer matrix (PTM) representation, and existing methods for learning a Pauli channel [13–15, 28] directly estimate each of its PTM's diagonal elements. Although the USI components $\overline{\mathcal{M}}_k$ are *not* diagonal in the PTM representation, our technique is also built around estimating the elements of the PTM.

The elements of $\overline{\mathcal{M}}_k$'s PTM $[\overline{\mathcal{M}}_k]_{P' \otimes Q_2, P \otimes Q_1} = \langle\langle P' \otimes Q_2 | \overline{\mathcal{M}}_k | P \otimes Q_1 \rangle\rangle$, where $P, P' \in \mathbb{P}_{n-m}$ and $Q_1, Q_2 \in \mathbb{P}_m$, are

$$\begin{aligned} [\overline{\mathcal{M}}_k]_{P' \otimes Q_2, P \otimes Q_1} &= \langle\langle P' \otimes Q_2 | \left(\sum_{a, b \in \mathbb{Z}_2^m} \mathcal{T}_{a, b} \otimes \mathcal{X}^{\otimes b} |k\rangle\langle k| \mathcal{X}^{\otimes a} \right) | P \otimes Q_1 \rangle\rangle \\ &= \langle\langle P' | \left(\sum_{a, b \in \mathbb{Z}_2^m} \mathcal{T}_{a, b} \right) | P \rangle\rangle \langle\langle Q_2 | \mathcal{X}^{\otimes b} |k\rangle\langle k| \mathcal{X}^{\otimes a} | Q_1 \rangle\rangle. \end{aligned} \quad (6)$$

Because $|k\rangle$ is a computational basis state, $\langle\langle k | \mathcal{X}^{\otimes a} | Q \rangle\rangle = 0$ for all $Q \in \mathbb{P}_m \setminus \mathbb{Z}_m$ and $a \in \mathbb{Z}_2^m$. Furthermore, because each $\mathcal{T}_{a, b}$ is a stochastic Pauli channel, $\langle\langle P' | \mathcal{T}_{a, b} | P \rangle\rangle = 0$ for all $P' \neq P$. Substituting these equalities into Eq. (6) and letting $Q_1 = Z^{\otimes d_1}$ and $Q_2 = Z^{\otimes d_2}$, we obtain $[\overline{\mathcal{M}}_k]_{P' \otimes Q_2, P \otimes Q_1} = 0$ when $P \neq P'$ and

$$[\overline{\mathcal{M}}_k]_{P \otimes Q_2, P \otimes Q_1} = \sum_{a, b \in \mathbb{Z}_2^m} \lambda_{a, b, P} (-1)^{(k \oplus a) \cdot d_1 + (k \oplus b) \cdot d_2} \quad (7)$$

$$= \sum_{a, b \in \mathbb{Z}_2^m} (-1)^{k \cdot (d_1 \oplus d_2)} (-1)^{(d_1 \cdot a) + (d_2 \cdot b)} \lambda_{a, b, P} \quad (8)$$

$$= (-1)^{k \cdot (d_1 \oplus d_2)} \tilde{\lambda}_{P, (Q_1, Q_2)}. \quad (9)$$

Here, $b_1 \oplus b_2$ denotes the bitwise XOR of $b_1, b_2 \in \mathbb{Z}_2^m$, and we have defined

$$\tilde{\lambda}_{P, \text{rest}, (Z^c, Z^d, Z^c)} = \sum_{a, b \in \mathbb{Z}_2^m} \lambda_{a, b} (-1)^{d \cdot b} (-1)^{a \cdot c + b \cdot c}. \quad (10)$$

Using Eq. (9), $\overline{\mathcal{M}}_k$ can be expressed in terms of its PTM elements as

$$\overline{\mathcal{M}}_k = \sum_P \sum_{Q_1, Q_2} (-1)^{k \cdot (d_1 \oplus d_2)} \tilde{\lambda}_{P, (Q_1, Q_2)} |P \otimes Q_2\rangle\langle P \otimes Q_1|. \quad (11)$$

Therefore, the $(P \otimes Q_1, P \otimes Q_2)$ PTM element of $\overline{\mathcal{M}}_k$ has value $\pm \tilde{\lambda}_{P, (Q_1, Q_2)}$ for all k , where the sign depends on the MCM result k .

Learning all $\tilde{\lambda}_{P, (Q_1, Q_2)}$ is sufficient to learn the USI. However, learning these values is complicated by the fact that $\overline{\mathcal{M}}_k$ is k -dependent and we cannot control which outcome k occurs. When $\overline{\mathcal{M}}$ is performed, it results in a uniformly random outcome k , so a uniformly random $\overline{\mathcal{M}}_k$ is applied to \mathcal{H} . If we apply $\overline{\mathcal{M}}$ to a Pauli operator $|P \otimes Q_1\rangle\rangle$ and simply ignore the measurement result, i.e., we trace over the classical register, we can measure

$$\sum_{k \in \mathbb{Z}_2^m} \langle\langle P \otimes Q_2 | \overline{\mathcal{M}} | P \otimes Q_1 \rangle\rangle = \sum_{k \in \mathbb{Z}_2^m} (-1)^{k \cdot (d_1 \oplus d_2)} \tilde{\lambda}_{P, (Q_1, Q_2)} \quad (12)$$

$$= \delta_{d_1, d_2} \tilde{\lambda}_{P, (Q_1, Q_2)}. \quad (13)$$

Therefore, without using MCM results, we can only learn the diagonal PTM elements $\tilde{\lambda}_{P,(Q,Q)}$.

To learn the remaining elements of $\overline{\mathcal{M}}$'s PTM, we incorporate the MCM results. An MCM result tells us the value of k , so we can compute the $(-1)^{k \cdot (d_1 \oplus d_2)}$ factors in the $\overline{\mathcal{M}}_k$ that occurred. We can then simulate measuring $(-1)^{k \cdot (d_1 \oplus d_2)} P \otimes Q_2$, by measuring $P \otimes Q_2$ and applying the sign in post-processing. This enables measuring

$$\langle\langle P \otimes Q_2 | (-1)^{k \cdot (d_1 \oplus d_2)} \overline{\mathcal{M}} | P \otimes Q_1 \rangle\rangle = \tilde{\lambda}_{P,(Q_1,Q_2)} \otimes \sum_{k \in \mathbb{Z}_2^n} |k\rangle. \quad (14)$$

We have shown that $\overline{\mathcal{M}}$ can be parameterized by $\{\tilde{\lambda}_{P,(Q_1,Q_2)}\}$, and that each $\tilde{\lambda}_{P,(Q_1,Q_2)}$ is either (a) a diagonal element of each $\overline{\mathcal{M}}_k$ that can be extracted without using MCM results, or (b) an off-diagonal element of each $\overline{\mathcal{M}}_k$ that can be extracted by applying a k -dependent sign in post-processing. These values are sufficient for complete reconstruction of $\overline{\mathcal{M}}$, but we may instead want to estimate $F(\overline{\mathcal{M}})$ or the rates of individual Pauli errors, which we can do by estimating the eigenvalues $\lambda_{a,b,P}$ of $\mathcal{T}_{a,b}$. For fixed P , the $\lambda_{P,(Q_1,Q_2)}$ are orthogonal linear combinations of $\{\lambda_{a,b,P}\}_{a,b \in \mathbb{Z}_2^n}$ [see the Supplemental Material (SM)] and can be used to determine individual eigenvalues $\lambda_{a,b,P}$ of any $\mathcal{T}_{a,b}$. In particular, the fidelity of $\overline{\mathcal{M}}$ is $\text{Tr}(\mathcal{T}_{0,0})$, and $\mathcal{T}_{0,0}$'s eigenvalues are

$$\lambda_{0,0,P_{\text{rest}}} = \frac{1}{4^m} \sum_{P_1, P_2 \in \mathbf{Z}_m} \tilde{\lambda}_{P_{\text{rest}},(P_1,P_2)}. \quad (15)$$

Therefore,

$$F(\overline{\mathcal{M}}) = \text{Tr}(\mathcal{T}_{0,0}) = \sum_{P_{\text{rest}} \in \mathbb{P}_{n-m}} \sum_{P_1, P_2 \in \mathbf{Z}_m} \tilde{\lambda}_{P_{\text{rest}},(P_1,P_2)}. \quad (16)$$

MCM cycle benchmarking—We now introduce *MCM cycle benchmarking (MCM-CB)*, which is a protocol for estimating the process fidelity of a randomly compiled MCM layer $\overline{\mathcal{M}}$. MCM-CB runs a random selection of Pauli noise learning subexperiments, each designed to learn a single parameter of $\overline{\mathcal{M}}$. An MCM-CB subexperiment is specified by an MCM layer L , an $(n-m)$ -qubit input Pauli operator P_{rest} , a pair of m -qubit Z -type Pauli operators (P_{meas}, Q) , a set of depths d , and a number of circuits per depth N . We require that L contains only Clifford gates on the $(n-m)$ unmeasured qubits (although note that techniques for CB of non-Clifford gates [30, 31] can be used to extend our method to the more general case). Furthermore, we require that d is even and $\mathcal{V}^d = \mathbb{I}$, where \mathcal{V} is the error-free evolution of the unmeasured subsystem specified by L .

An MCM-CB subexperiment is the following procedure:

1. For each depth d , generate N MCM-CB circuits $C = L_0 \overline{L}^d L_f$ (read left to right), where
 - (a) L_0 is a layer of single-qubit gates preparing a random tensor product eigenstate of $P_{\text{rest}} \otimes Z^{\otimes m}$,
 - (b) \overline{L} is the layer L with randomized compiling, and

- (c) L_f is a layer of single-qubit gates that transforms P_{rest} into a Z -type Pauli $Z^{\otimes t_f}$.

When C is implemented without errors, measuring $Z^{\otimes t_f}$ always gives $(-1)^{t_0}$, where $t_0 \in \mathbb{Z}_2$.

2. Run each circuit C and compute

$$f(C) = (-1)^{t_f \cdot b_f + t_0} \prod_{i=1}^d (-1)^{b_i \cdot t_{\text{mcm}}}, \quad (17)$$

where t_{mcm} is defined by $P_{\text{meas}} Q = Z^{\otimes t_{\text{mcm}}}$, b_f is the n -bit final measurement outcome, and b_i is the m -bit MCM outcome from layer i . Eq. (17) assumes that the classical postprocessing of MCM outcomes specified by the randomized compilation procedure has already been applied to b_i .

3. Compute $\overline{f}_d = \frac{1}{N} \sum_{j=1}^N f(C_j)$, and fit \overline{f}_d to

$$\overline{f}_d = A P_{\text{rest},(P_{\text{meas}},Q)}^d. \quad (18)$$

The result of an MCM-CB subexperiment is an estimate $\hat{P}_{\text{rest},(P_{\text{meas}},Q)}$ of a quantity $p_{P_{\text{rest},(P_{\text{meas}},Q)}}$ that is determined by the PTM elements $\tilde{\lambda}_{P,(Q_1,Q_2)}$ of $\overline{\mathcal{M}}$, where $\overline{\mathcal{M}} = \overline{\mathcal{M}}(\mathcal{V} \otimes \mathbb{I}_m)$. Specifically, $\hat{P}_{\text{rest},(P_{\text{meas}},Q)} \approx p_{P_{\text{rest},(P_{\text{meas}},Q)}}$, where

$$p_{P_{\text{rest},(P_{\text{meas}},Q)}} = \sqrt{\prod_{j=1}^{\ell} \tilde{\lambda}_{\mathcal{V}^j[P_1,(Q^{j-1}P_{\text{meas}},Q^jP_{\text{meas}})]}}, \quad (19)$$

and where ℓ is the smallest positive even integer satisfying $\mathcal{V}^\ell = \mathbb{I}_{n-m}$, as long as $\tilde{\lambda}_{\mathcal{V}^j[P_1,(Q^{j-1}P_{\text{meas}},Q^jP_{\text{meas}})]} > \delta$ for some constant $\delta > 0$ for all $1 \leq j \leq \ell$. An MCM-CB subexperiment can be thought of as an experiment to estimate a specific parameter of a USI, determined by Eq. (19). Additionally, one MCM-CB circuit set can be used to estimate $\hat{P}_{\text{rest},(P_{\text{meas}},Q)}$ for all $(P_{\text{rest}}, Q) \in \mathbf{Z}_m \times \mathbf{Z}_m$, because the circuits are fully determined by P_{rest} . These $\hat{P}_{\text{rest},(P_{\text{meas}},Q)}$ can be used to estimate $\lambda_{a,b,P_{\text{rest}}}$ by making the assumption $p_{P_{\text{rest},(P_{\text{meas}},Q)}} \approx \tilde{\lambda}_{P_{\text{rest}},(Q,P_{\text{meas}})}$.

The MCM-CB protocol consists of running many MCM-CB subexperiments to estimate the fidelity of $\overline{\mathcal{M}}$. Our protocol is the following:

1. Pick K uniformly random triplets of Pauli operators $(P_{\text{rest}}, P_{\text{meas}}, Q) \in \mathbb{P}_{n-m} \times \mathbf{Z}_m \times \mathbf{Z}_m$.
2. For each triplet of Pauli operators $(P_{\text{rest},k}, P_{\text{meas},k}, Q_k)$, perform an MCM-CB subexperiment with input Pauli P_k and measured subsystem Paulis $(P_{\text{meas},k}, Q_k)$, and estimate the decay constant $\hat{P}_{\text{rest},k,(P_{\text{meas},k},Q_k)}$.
3. Compute the estimated process fidelity,

$$\hat{F} = \frac{1}{K} \sum_{k=1}^K \hat{P}_{\text{rest},k,(P_{\text{meas},k},Q_k)}. \quad (20)$$

When $m = 0$, this protocol reduces to CB of Clifford gates. The number of samples K required for MCM-CB to estimate F to within a fixed multiplicative uncertainty is independent of n , so our method remains sample efficient for large n (see the SM).

The fidelity of randomly compiled MCMs—In the infinite sampling limit, MCM-CB measures $F_{\text{MCM-CB}}$, and this value satisfies $F_{\text{MCM-CB}} \leq F(\overline{\mathcal{M}})$. This is because MCM-CB estimates $F(\overline{\mathcal{M}})$ by averaging the MCM-CB decay constants $p_{P_{\text{rest}},(P_{\text{rest}},Q)}$, many of which are the geometric mean of multiple $\tilde{\lambda}_{P_{\text{rest}},(P_{\text{rest}},Q)}$ [Eq. (19)]. MCM-CB uses the approximation

$$\sqrt{\prod_{k=1}^{\ell} \tilde{\lambda}_{V^k[P],(Q^{k-1}P_{\text{meas}},Q^kP_{\text{meas}})}} \approx \frac{1}{\ell} \sum_{k=1}^{\ell} \tilde{\lambda}_{V^k[P],(Q^{k-1}P_{\text{meas}},Q^kP_{\text{meas}})}. \quad (21)$$

In the SM, we show that this approximation implies that $F_{\text{MCM-CB}} \leq F(\overline{\mathcal{M}})$.

The result of CB of Clifford gates is often used as an estimate of the fidelity of the bare Clifford layer—i.e., the layer *without* randomized compiling—and this is reliable because randomized compiling of Clifford gates preserves process fidelity (when single-qubit gates are perfect). However, randomized compiling does *not* preserve the fidelity of MCM layers. Instead, $F(\overline{\mathcal{M}}) \leq F(\mathcal{M})$ for any instrument \mathcal{M} . The fidelity of the randomly compiled instrument is (using Eq. (46) in Ref. [27])

$$F(\overline{\mathcal{M}}) = \text{Tr} \left(\mathbb{E}_{G \in \mathbb{P}_{n-m}} \mathbb{E}_{k \in \mathbb{Z}_2^n} (G^\dagger V^\dagger \otimes \langle\langle k | \rangle\rangle \mathcal{M}_k(G \otimes |k\rangle\langle\langle k | \rangle)) \right) \quad (22)$$

$$= \frac{1}{2^m} \sum_{k \in \mathbb{Z}_2^m} \text{Tr} \left(\mathcal{M}_k(V^\dagger \otimes |k\rangle\langle\langle k | \rangle) \right). \quad (23)$$

Comparing Eq. (23) to Eq. (3), we conclude that $F(\overline{\mathcal{M}}) \leq F(\mathcal{M})$ for all \mathcal{M} .

Simulations—We simulated MCM-CB of layers consisting of computational basis measurements and idle gates, using Stim [32]. We randomly sampled USIs of the form $\mathcal{M} = \mathcal{E}_{\text{post}}(\mathcal{T} \otimes \mathbb{I}_{n-m})\mathcal{L}\mathcal{E}_{\text{pre}}$, where \mathcal{L} is the error-free quantum instrument, \mathcal{T} is a stochastic Pauli channel acting on the unmeasured qubits, and \mathcal{E}_{pre} and $\mathcal{E}_{\text{post}}$ are n -qubit stochastic Pauli error channels where each Pauli error acts nontrivially on at least one measured qubit. We sampled 3^{n-m} uniform random Pauli error rates for each \mathcal{E}_{pre} and $\mathcal{E}_{\text{post}}$, and normalize them such that the total error rate is $p/2$. Each \mathcal{T} has 3^{n-m} Pauli error rates sampled equivalently, with total error rate p . We sampled 120 error models with $p \in [0.0001, 0.0601]$. We model initial state preparation and final measurement error as independent bit flip errors on each qubit, and we sample each qubit’s error rate at random such that the average state preparation (measurement) error rate per qubit is 0.005 (0.01).

We simulated MCM-CB with $K = 100$ sampled Paulis and layers with $n - m = 4, 6, 8$ unmeasured (idling) qubits and $m = 1, 2$ measurements. Figure 2a shows the MCM-CB estimates of the process fidelity (all error bars are 1σ and computed via a parametric bootstrap). We observe that for these

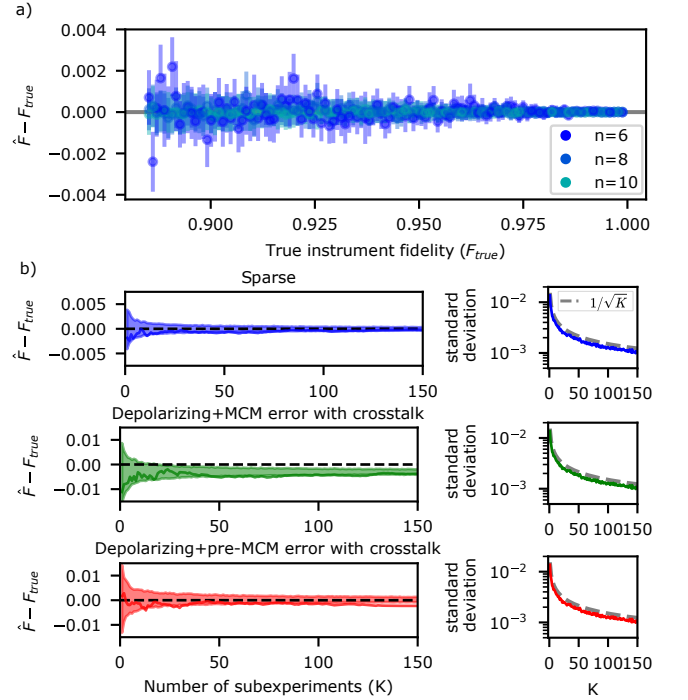


FIGURE 2. **Simulating MCM-CB on up to 10 qubits.** (a) MCM-CB of $m = 2$ measured qubits and $n - m = 4, 6, 8$ idling qubits with randomly generated USI error models. The MCM-CB estimate is accurate for all error models. (b) Convergence of the MCM-CB fidelity estimate (solid line, with shaded region showing $\pm 1\sigma$ region) with the number of subexperiments (K) for three USI error models with $n = 5$ and $m = 2$ qubits, computed by sampling K MCM-CB decay parameters 400 times. The standard deviation of \hat{F} scales with $1/\sqrt{K}$.

error models, MCM-CB accurately estimates the USI’s process fidelity. The uncertainty in the MCM-CB estimates is small for all error models. Most estimates lie within 1σ of the true fidelity, and all lie within 2.5σ . Figure 2c shows how the standard deviation of \hat{F} scales with K for simulated MCM-CB experiments with $n = 7$ qubits and $m = 2$ measured qubits (see the SM for details). The standard deviation decreases quickly with K , and it has the expected $1/\sqrt{K}$ scaling for CB [28].

While MCM-CB is very accurate for the error models used in Fig. 2a, it is only expected to reliably lower-bound the process fidelity, rather than accurately estimate the fidelity, for general error models. We expect to see larger deviations from the true fidelity with USIs that have low fidelity, and where many of the $\tilde{\lambda}_{P,(Q_1,Q_2)}$ differ in magnitude from $\tilde{\lambda}_{P,(Q_2,Q_1)}$ (e.g., because of high rates of correlated pre- or post-MCM error, or error that is strongly biased towards pre- or post-MCM error). We show additional simulation results in the SM that explore this effect.

IBM Q demonstrations—We ran MCM-CB on `ibm_osaka` to benchmark an $n = 4$ qubit layer of linearly-connected qubits (Q40–Q43) with $m = 1$ MCMs (on Q40), and $n - m = 3$ idling qubits that have X-X dynamical decoupling applied. We exhaustively sample the MCM-CB subexperiments, which requires running 64 sets of MCM-CB circuits and performing

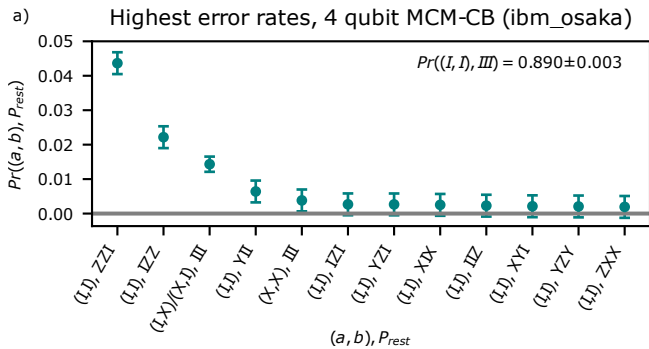


FIGURE 3. **MCM-CB on 4 qubits of an IBM Q processor.** The 12 largest Pauli error rates for a 4-qubit layer of one MCM and three idling qubits on `ibm_osaka`. Only 5 error rates are more than 1σ greater than 0. The dominant errors are ZZ errors on adjacent idling qubits and single bit flip errors on the measured qubit.

4 different analyses of each circuit set [33]. See the SM for full results.

Figure 1c shows the estimated infidelity of the full 4-qubit layer and its subsets (obtained by data marginalization). The errors on the unmeasured subsystem are much larger than the errors on the measured qubit—the measured qubit’s infidelity [0.022(2)] is low relative to the infidelity of the individual idling qubits [0.072(8), 0.085(8), and 0.040(5)]. The infidelity of the whole idling subsystem [0.11(1)] is only slightly higher than the infidelity of the highest-error individual qubits, indicating predominately correlated errors. The infidelity of the idling subsystem [0.10(1)] is within 1σ of the infidelity of the full 4-qubit cycle.

To obtain more details of the error, we estimate the Pauli error probabilities for each $\mathcal{T}_{a,b}$. We do this by estimating $\lambda_{0,0,P_{rest}}$, $\lambda_{1,1,P_{rest}}$, and $\lambda_{0,1,P_{rest}} + \lambda_{1,0,P_{rest}}$ for all $P_{rest} \in \mathbb{P}_3$ and performing a Walsh-Hadamard transform [14] on each of these three sets of Pauli eigenvalues. We use the approximation $\tilde{\lambda}_{P_{rest},(I,Z)} = \tilde{\lambda}_{P_{rest},(Z,I)} = \hat{p}_{P_{rest},(I,Z)}$ to estimate $\lambda_{0,0,P_{rest}}$ and $\lambda_{1,1,P_{rest}}$ (see the SM for details). Figure 3 shows the dominant Pauli errors. All but 5 error rates are within 1σ of 0. The dominant errors are ZZ errors on adjacent idling qubits [probabilities 0.044(3) and 0.022(3)], which is consistent with the known coherent error caused by ZZ coupling in transmon qubits [34]. The next largest source of error is single bit flip errors on the measured qubit, which happen with probability 0.014(2).

MCM layer set cycle benchmarking—MCM-CB of a single MCM layer can learn a limited number of parameters of the layer’s error. To learn more parameters of a USI, we can benchmark a *set* of layers containing multi-qubit Clifford gates and MCM layers. To do so, it is useful to also extend MCM-CB to allow arbitrary single-qubit gates between repetitions of a layer (analogous to Ref. [16]), rather than just the Pauli gates required for randomized compilation. This enables freely transforming between Pauli operators with the same support, in which case the learnable parameters of a layer set are determined by the cycle space of the layer set’s *pattern transfer graph* (PTG), which describes how each layer transforms the support $\text{supp}(P)$ of Pauli opera-

tors [16]. To include MCM layers in the PTG, we add an edge from $\text{supp}(P_{rest} \otimes P_{meas})$ to $\text{supp}(P_{rest} \otimes Q)$ for each USI PTG element $\tilde{\lambda}_{P_{rest},(P_{meas},Q)}$. There is an (extended) MCM-CB subexperiment that learns a product of parameters iff that product is a composition of cycles in the PTG. These MCM-CB subexperiments use a repeated *sequence* of layers from the layer set. For example, by performing MCM-CB subexperiments with the sequence of 2-qubit layers consisting of a controlled Z gate followed by a single-qubit MCM, we can learn 12 parameters that cannot be learned by separately characterizing the two layers. Each of these parameters is a relational quantity that depends on the error of both layers (see the SM for details).

Discussion—We have introduced theory for comprehensively characterizing USI error, by extending Pauli noise learning to MCMs. Furthermore, we have introduced MCM-CB, a scalable protocol for estimating the process fidelity of a randomly compiled MCM layer and for lower bounding the process fidelity of the layer without randomized compiling. We have also demonstrated how our method can be used to obtain detailed error information for MCM layers on current quantum processors.

MCM-CB enables detecting and quantifying measurement crosstalk and correlated error in MCM layers, which can provide useful diagnostic information. Accurate Pauli noise learning is also critical to the performance of common error mitigation techniques [18, 20]. Our method is capable of learning more details of MCM noise than existing noise learning techniques for measurements [20, 25], and can therefore be applied to improve the accuracy of error models for use in error mitigation. Our theory can also potentially extend to learning the error present in MCMs with classical feedforward in detail [20].

While we have focused on characterizing individual MCM cycles, some of the most interesting applications of our theory are extending other Pauli noise learning techniques [14, 17] to benchmark complex circuits or layer sets containing MCMs. In particular, we anticipate our method will be integrated with existing MCM-free Pauli noise learning techniques for characterizing syndrome extraction circuits [21, 22].

Note—After the completion of this work, Ref. [35] was posted to arXiv, which introduces a similar Pauli noise learning method to ours.

ACKNOWLEDGEMENTS

This material was funded in part by the U.S. Department of Energy, Office of Science, Office of Advanced Scientific Computing Research, Quantum Testbed Pathfinder Program. T.P. acknowledges support from an Office of Advanced Scientific Computing Research Early Career Award. Sandia National Laboratories is a multi-program laboratory managed and operated by National Technology and Engineering Solutions of Sandia, LLC., a wholly owned subsidiary of Honeywell International, Inc., for the U.S. Department of Energy’s National Nuclear Security Administration under contract DE-

NA-0003525. We acknowledge the use of IBM Quantum services for this work. All statements of fact, opinion or conclusions contained herein are those of the authors and should not be construed as representing the official views or policies of the U.S. Department of Energy, or the U.S. Government, or IBM, or the IBM Quantum team.

REFERENCES

- [1] Earl T Campbell, Barbara M Terhal, and Christophe Vuillot, “Roads towards fault-tolerant universal quantum computation,” *Nature* **549**, 172–179 (2017).
- [2] Google Quantum AI, “Suppressing quantum errors by scaling a surface code logical qubit,” *Nature* **614**, 676–681 (2023).
- [3] Dolev Bluvstein, Simon J Evered, Alexandra A Geim, Sophie H Li, Hengyun Zhou, Tom Manovitz, Sepehr Ebadi, Madelyn Cain, Marcin Kalinowski, Dominik Hangleiter, J Pablo Bonilla Ataides, Nishad Maskara, Iris Cong, Xun Gao, Pedro Sales Rodriguez, Thomas Karolyshyn, Giulia Semeghini, Michael J Gullans, Markus Greiner, Vladan Vuletić, and Mikhail D Lukin, “Logical quantum processor based on reconfigurable atom arrays,” *Nature* (2023), 10.1038/s41586-023-06927-3.
- [4] Sebastian Krinner, Nathan Lacroix, Ants Remm, Agustin Di Paolo, Elie Genois, Catherine Leroux, Christoph Hellings, Stefania Lazar, Francois Swiadek, Johannes Herrmann, Graham J Norris, Christian Kraglund Andersen, Markus Müller, Alexandre Blais, Christopher Eichler, and Andreas Wallraff, “Realizing repeated quantum error correction in a distance-three surface code,” *Nature* **605**, 669–674 (2022).
- [5] Riddhi S Gupta, Neereja Sundaresan, Thomas Alexander, Christopher J Wood, Seth T Merkel, Michael B Healy, Marius Hillenbrand, Tomas Jochym-O’Connor, James R Wootton, Theodore J Yoder, Andrew W Cross, Maika Takita, and Benjamin J Brown, “Encoding a magic state with beyond break-even fidelity,” *Nature* **625**, 259–263 (2024).
- [6] Tsung-Cheng Lu, Leonardo A. Lessa, Isaac H. Kim, and Timothy H. Hsieh, “Measurement as a shortcut to long-range entangled quantum matter,” *PRX Quantum* **3**, 040337 (2022).
- [7] Robert B. Griffiths and Chi-Sheng Niu, “Semiclassical fourier transform for quantum computation,” *Phys. Rev. Lett.* **76**, 3228–3231 (1996).
- [8] Elisa Bäumer, Vinay Tripathi, Derek S. Wang, Patrick Rall, Edward H. Chen, Swarnadeep Majumder, Alireza Seif, and Zlatko K. Minev, “Efficient long-range entanglement using dynamic circuits,” (2023), arXiv:2308.13065 [quant-ph].
- [9] Kenneth Rudinger, Guilhem J. Ribeill, Luke C.G. Govia, Matthew Ware, Erik Nielsen, Kevin Young, Thomas A. Ohki, Robin Blume-Kohout, and Timothy Proctor, “Characterizing midcircuit measurements on a superconducting qubit using gate set tomography,” *Phys. Rev. Appl.* **17**, 014014 (2022).
- [10] Roman Stricker, Davide Vodola, Alexander Erhard, Lukas Postler, Michael Meth, Martin Ringbauer, Philipp Schindler, Rainer Blatt, Markus Müller, and Thomas Monz, “Characterizing quantum instruments: From nondemolition measurements to quantum error correction,” *PRX Quantum* **3**, 030318 (2022).
- [11] L C G Govia, P Jurcevic, C J Wood, N Kanazawa, S T Merkel, and D C McKay, “A randomized benchmarking suite for mid-circuit measurements,” *New Journal of Physics* **25**, 123016 (2023).
- [12] J. P. Gaebler, C. H. Baldwin, S. A. Moses, J. M. Dreiling, C. Figgatt, M. Foss-Feig, D. Hayes, and J. M. Pino, “Suppression of midcircuit measurement crosstalk errors with micromotion,” *Phys. Rev. A* **104**, 062440 (2021).
- [13] Steven T. Flammia and Joel J. Wallman, “Efficient estimation of pauli channels,” *ACM Transactions on Quantum Computing* **1**, 1–32 (2020).
- [14] Robin Harper, Steven T. Flammia, and Joel J. Wallman, “Efficient learning of quantum noise,” *Nature Physics* **16**, 1184–1188 (2020).
- [15] Robin Harper, Wenjun Yu, and Steven T. Flammia, “Fast estimation of sparse quantum noise,” *PRX Quantum* **2**, 010322 (2021).
- [16] Senrui Chen, Yunchao Liu, Matthew Otten, Alireza Seif, Bill Fefferman, and Liang Jiang, “The learnability of Pauli noise,” *Nature Communications* **14**, 52 (2023), publisher: Nature Publishing Group.
- [17] Steven T. Flammia, “Averaged circuit eigenvalue sampling,” (Schloss Dagstuhl – Leibniz-Zentrum für Informatik, 2022).
- [18] Kristan Temme, Sergey Bravyi, and Jay M. Gambetta, “Error mitigation for short-depth quantum circuits,” *Phys. Rev. Lett.* **119**, 180509 (2017).
- [19] Ewout van den Berg, Zlatko K. Minev, Abhinav Kandala, and Kristan Temme, “Probabilistic error cancellation with sparse pauli-lindblad models on noisy quantum processors,” *Nature Physics* **19**, 1116–1121 (2023).
- [20] Riddhi S. Gupta, Ewout van den Berg, Maika Takita, Diego Riste, Kristan Temme, and Abhinav Kandala, “Probabilistic error cancellation for dynamic quantum circuits,” (2023), arXiv:2310.07825 [quant-ph].
- [21] Robin Harper and Steven T. Flammia, “Learning correlated noise in a 39-qubit quantum processor,” *PRX Quantum* **4**, 040311 (2023).
- [22] Evan T. Hockings, Andrew C. Doherty, and Robin Harper, “Scalable noise characterisation of syndrome extraction circuits with averaged circuit eigenvalue sampling,” (2024), arXiv:2404.06545 [quant-ph].
- [23] Joel J. Wallman and Joseph Emerson, “Noise tailoring for scalable quantum computation via randomized compiling,” *Phys. Rev. A* **94**, 052325 (2016).
- [24] Stefanie J. Beale and Joel J. Wallman, “Randomized compiling for subsystem measurements,” (2023), arXiv:2304.06599 [quant-ph].
- [25] Akel Hashim, Arnaud Carignan-Dugas, Larry Chen, Christian Juenger, Neelay Fruitwala, Yilun Xu, Gang Huang, Joel J. Wallman, and Irfan Siddiqi, “Quasi-probabilistic readout correction of mid-circuit measurements for adaptive feedback via measurement randomized compiling,” (2024), arXiv:2312.14139 [quant-ph].
- [26] Darian McLaren, Matthew A. Graydon, and Joel J. Wallman, “Stochastic errors in quantum instruments,” (2023), arXiv:2306.07418 [quant-ph].
- [27] Stefanie J. Beale and Joel J. Wallman, “Randomized compiling for subsystem measurements,” (2023), arXiv:2304.06599 [quant-ph].
- [28] Alexander Erhard, Joel J. Wallman, Lukas Postler, Michael Meth, Roman Stricker, Esteban A. Martinez, Philipp Schindler, Thomas Monz, Joseph Emerson, and Rainer Blatt, “Characterizing large-scale quantum computers via cycle benchmarking,” *Nature Communications* **10** (2019), 10.1038/s41467-019-13068-7.
- [29] Arnaud Carignan-Dugas, Shashank Kumar Ranu, and Patrick Dreher, “Estimating Coherent Contributions to the Error Profile Using Cycle Error Reconstruction,” (2023), arXiv:2303.09945 [quant-ph].

- [30] Yosep Kim, Alexis Morvan, Long B. Nguyen, Ravi K. Naik, Christian Jünger, Larry Chen, John Mark Kreikebaum, David I. Santiago, and Irfan Siddiqi, “High-fidelity three-qubit itofoli gate for fixed-frequency superconducting qubits,” *Nature Physics* **18**, 783–788 (2022).
- [31] Akel Hashim, Rich Rines, Victory Omole, Ravi K. Naik, John Mark Kreikebaum, David I. Santiago, Frederic T. Chong, Irfan Siddiqi, and Pranav Gokhale, “Optimized swap networks with equivalent circuit averaging for qaoa,” *Phys. Rev. Res.* **4**, 033028 (2022).
- [32] Craig Gidney, “Stim: a fast stabilizer circuit simulator,” *Quantum* **5**, 497 (2021).
- [33] Note that $p_{P_{\text{rest}},(I,Z)} = p_{P_{\text{rest}},(Z,I)}$ for the MCM layer we benchmarked, and therefore only 3 analyses are strictly required for each circuit set. We performed both of the equivalent analyses and observed $p_{P_{\text{rest}},(I,Z)} = p_{P_{\text{rest}},(Z,I)}$ for all P_{rest} .
- [34] Vinay Tripathi, Huo Chen, Mostafa Khezri, Ka-Wa Yip, E.M. Levenson-Falk, and Daniel A. Lidar, “Suppression of crosstalk in superconducting qubits using dynamical decoupling,” *Phys. Rev. Appl.* **18**, 024068 (2022).
- [35] Zhihan Zhang, Senrui Chen, Yunchao Liu, and Liang Jiang, “A generalized cycle benchmarking algorithm for characterizing mid-circuit measurements,” (2024), [arXiv:2406.02669](https://arxiv.org/abs/2406.02669) [quant-ph].

SUPPLEMENTAL MATERIAL

I. MCM-CB THEORY

A. MCM-CB with Clifford Gates on Unmeasured Qubits

In the main text, we assume that the error-free evolution of the unmeasured subsystem is $\mathcal{V} = \mathbb{I}_{n-m}$. We obtain the general case, i.e., \mathcal{V} is any $(n-m)$ -qubit Clifford operation, by decomposing $\overline{\mathcal{M}} = \overline{\mathcal{M}'}(\mathcal{V} \otimes \mathbb{I}_m)$, where $\overline{\mathcal{M}'}$ is a USI with ideal evolution \mathbb{I}_{n-m} on the unmeasured subsystem, i.e.,

$$\overline{\mathcal{M}'}_k = \sum_{a,b \in \mathbb{Z}_2^m} \mathcal{T}_{a,b} \otimes \mathcal{X}^{\otimes b} |k\rangle\langle k| \mathcal{X}^{\otimes a}. \quad (24)$$

The PTM elements of $\overline{\mathcal{M}}$ are given by

$$\langle\langle P' \otimes Q_2 | \overline{\mathcal{M}}_k | P \otimes Q_1 \rangle\rangle = \langle\langle P' \otimes Q_2 | \overline{\mathcal{M}'}_k | \mathcal{V}[P] \otimes Q_1 \rangle\rangle. \quad (25)$$

Because $\mathcal{V}[P]$ is also a Pauli operator, we can now apply Eq. (9), and the rest of our theory follows.

B. Estimating the Process Fidelity of USIs

In this section, we show that all $\tilde{\lambda}_{P_{\text{rest}},(P_{\text{meas}},Z^d P_{\text{meas}})}$ are linearly independent. We show that any two distinct $\tilde{\lambda}_{P_{\text{rest}},(P_{\text{meas}},Z^d P_{\text{meas}})}$ are orthogonal linear combinations of $\{\lambda_{a,b}\}_{a,b \in \mathbb{Z}_2^m}$ by (1) expressing each $\tilde{\lambda}_{P_{\text{rest}},(P_{\text{meas}},Z^d P_{\text{meas}})}$ as a 2^m -dimensional vector $\vec{v}_{P_{\text{rest}},(P_{\text{meas}},Z^d P_{\text{meas}})}$ in the basis $\{\lambda_{a,b}\}_{a,b \in \mathbb{Z}_2^m}$, and (2) taking a dot product of the resulting vectors for two parameters $\tilde{\lambda}_{P_{\text{rest}},(Z^c, Z^d Z^c)}$ and $\tilde{\lambda}_{P_{\text{rest}},(Z^{c'}, Z^{d'} Z^{c'})}$:

$$\vec{v}_{P_{\text{rest}},(Z^c, Z^d Z^c)} \cdot \vec{v}_{P_{\text{rest}},(Z^{c'}, Z^{d'} Z^{c'})} = \sum_{a,b} (-1)^{b \cdot d} (-1)^{b \cdot d'} (-1)^{(a \oplus b) \cdot c} (-1)^{(a \oplus b) \cdot c'} \quad (26)$$

$$= \sum_{a,b} (-1)^{b \cdot (d \oplus d')} (-1)^{(a \oplus b) \cdot (c \oplus c')} \quad (27)$$

$$= \delta_{d,d'} \delta_{c,c'}, \quad (28)$$

where δ denotes the Kronecker delta. To obtain an expression for $\lambda_{0,0,P_{\text{rest}}}$, we sum over $\tilde{\lambda}_{P_{\text{rest}},(Z^c, Z^d Z^c)}$ for all $d, c \in \mathbf{Z}_m$:

$$\sum_{d,c \in \mathbb{Z}_2^m} \tilde{\lambda}_{P_{\text{rest}},(Z^c, Z^d Z^c)} = \sum_{d,c \in \mathbb{Z}_2^m} \sum_{a,b \in \mathbb{Z}_2^m} \lambda_{a,b} (-1)^{d \cdot b} (-1)^{c \cdot a + c \cdot b} \quad (29)$$

$$= \sum_{d \in \mathbb{Z}_2^m} \sum_{a,b \in \mathbb{Z}_2^m} \lambda_{a,b} (-1)^{d \cdot b} \delta_{a,b} \quad (30)$$

$$= \sum_{a \in \mathbb{Z}_2^m} \sum_{d \in \mathbb{Z}_2^m} \lambda_{a,a} (-1)^{d \cdot a} \quad (31)$$

$$= \lambda_{0,0,P_{\text{rest}}}. \quad (32)$$

Eq (16) follows by summing over all $P_{\text{rest}} \in \mathbb{P}_{n-m}$

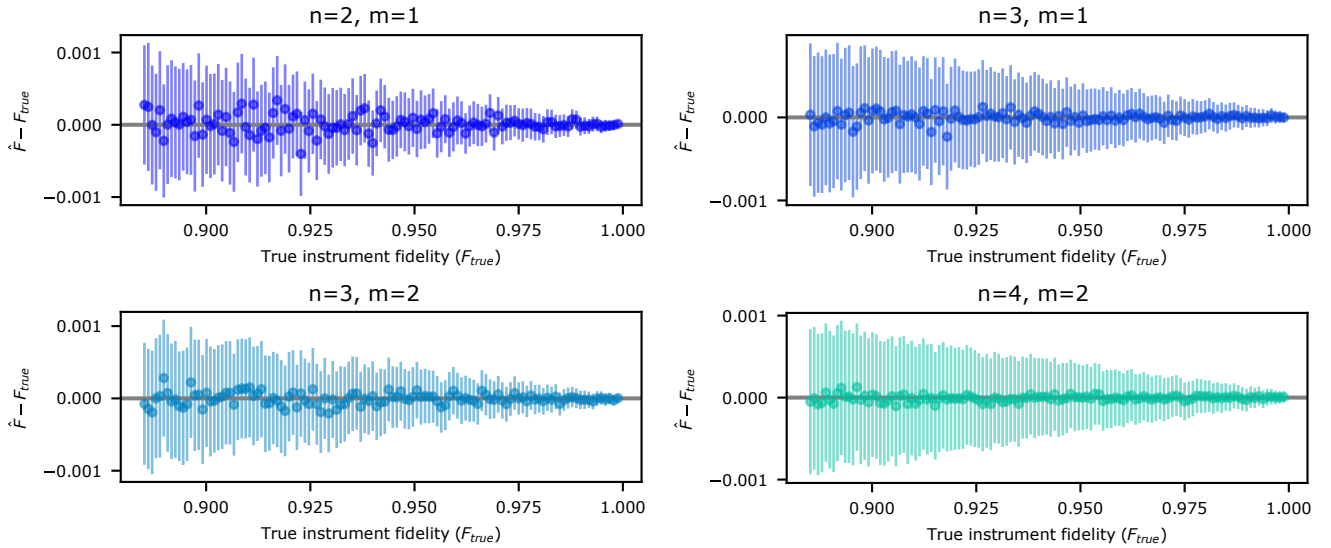


FIGURE 4. **Simulating MCM-CB on 2-4 qubits.** The absolute error of MCM-CB fidelity estimates from simulations of MCM-CB with $m = 1, 2$ measured qubits and $n - m = 1, 2$ idling qubits, using randomly generated USI error models. The MCM-CB estimate is highly accurate for all error models, and the uncertainty is small.

C. Process Fidelity and Cycle Benchmarking

Here, we show that the infinite-sampling limit MCM-CB result $F_{\text{MCM-CB}}$ is a lower bound on $F(\overline{\mathcal{M}})$. MCM-CB is a lower bound on $F(\overline{\mathcal{M}})$. In the limit of sampling all of the possible MCM-CB subexperiments, the MCM-CB fidelity estimate consists of averaging over all MCM-CB decay constants for a given cycle. The result of this averaging (using the true values of the decay constants), is

$$F_{\text{MCM-CB}} = \frac{1}{4^n} \sum_{P \in \mathbb{P}_{n-m}} \sum_{P_{\text{meas}} \in \mathcal{Z}_m} \sum_{Q \in \mathcal{Z}_m} \sqrt{\prod_{k=1}^{\ell} \tilde{\lambda}_{\mathcal{V}^k[P], (Q^{k-1}P_{\text{meas}}, Q^k P_{\text{meas}})}} \quad (33)$$

$$\leq \frac{1}{4^n} \sum_{P \in \mathbb{P}_{n-m}} \sum_{P_{\text{meas}} \in \mathcal{Z}_m} \sum_{Q \in \mathcal{Z}_m} \frac{1}{\ell} \sum_{k=1}^{\ell} \tilde{\lambda}_{\mathcal{V}^k[P], (Q^{k-1}P_{\text{meas}}, Q^k P_{\text{meas}})} \quad (34)$$

$$\leq \frac{1}{4^n} \sum_{P \in \mathbb{P}_{n-m}} \sum_{Q_1, Q_2 \in \mathcal{Z}_m} \frac{1}{\ell} \sum_{k=1}^{\ell/2} (\tilde{\lambda}_{\mathcal{V}^{2k-1}[P], (Q_1, Q_2)} + \tilde{\lambda}_{\mathcal{V}^{2k}[P], (Q_2, Q_1)}) \quad (35)$$

$$\leq \frac{1}{4^n} \sum_{P \in \mathbb{P}_{n-m}} \frac{1}{\ell} \sum_{k=1}^{\ell/2} (\lambda_{0,0,\mathcal{V}^{2k-1}[P], (Q_1, Q_2)} + \lambda_{0,0,\mathcal{V}^{2k}[P], (Q_2, Q_1)}) \quad (36)$$

$$\leq \frac{1}{4^n} \sum_{P \in \mathbb{P}_{n-m}} \lambda_{0,0,P}. \quad (37)$$

This result implies that $F_{\text{MCM-CB}} \leq F(\overline{\mathcal{M}})$ for any USI $\overline{\mathcal{M}}$.

II. MCM-CB SIMULATIONS

A. Simulations of MCM-CB on up to 4 Qubits

In the few-qubit limit, it is feasible to perform every possible MCM-CB subexperiment, and this is often done in practice for CB of two-qubit gates. We simulated MCM-CB with this exhaustive sampling for USIs with $n - m = 1, 2$ unmeasured qubits and $m = 1, 2$ measurements. We simulated our method with randomly sampled USIs $\overline{\mathcal{M}} = \mathcal{E}_{\text{post}}(\mathcal{T} \otimes \mathbb{I}_{n-m})\mathcal{L}\mathcal{E}_{\text{pre}}$. We sampled these USIs so that the infidelity of \mathcal{T} is p and the infidelity of \mathcal{E}_{pre} and $\mathcal{E}_{\text{post}}$ are $p/2$, for 120 uniformly-spaced values $p \in [0.0001, 0.0601)$. For each stochastic error channel, the Pauli error rates are chosen uniformly, and then rescaled to

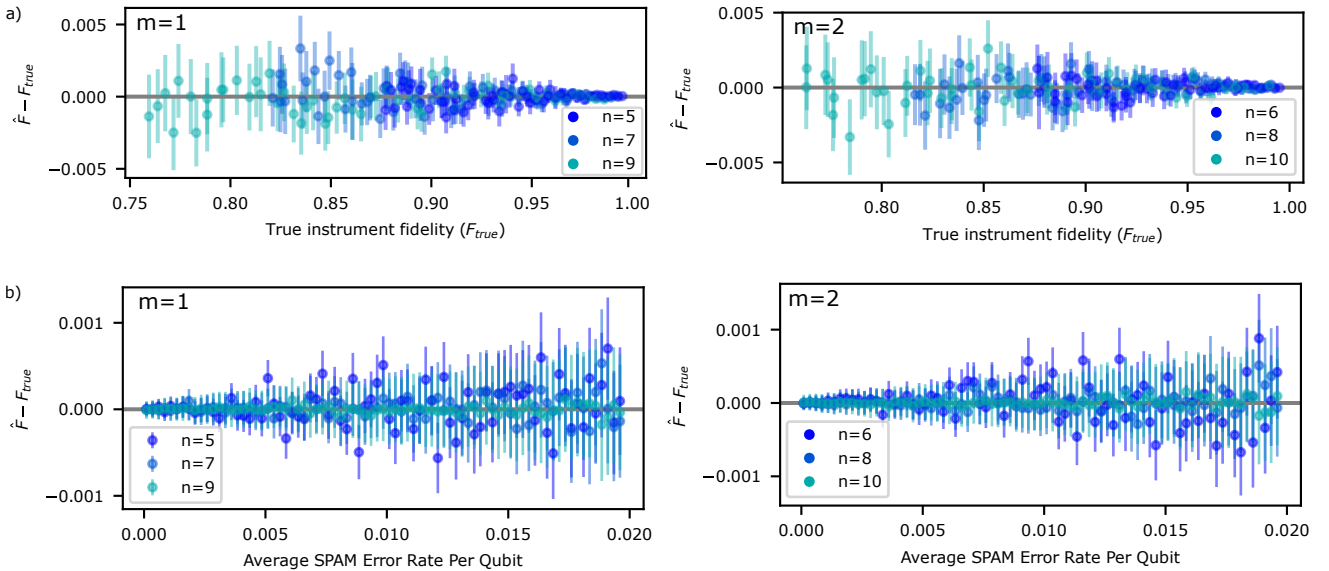


FIGURE 5. **Simulating MCM-CB with additional error models.** (a) The absolute error in fidelity estimates from simulated MCM-CB with models consisting of (1) local depolarizing error on each unmeasured qubit, which is independent of error on the measured qubits, and (2) crosstalk errors that include the measured qubits and unmeasured qubits. The MCM-CB estimate is accurate for all error models, with increasing estimate uncertainty with decreasing fidelity. (b) The absolute error in fidelity estimates from simulated MCM-CB with an MCM layer with fidelity 0.94 and varied rates of initial state preparation and final measurement error. MCM-CB remains accurate for models with average bit flip error rates of up to 2% per qubit.

obtain a stochastic Pauli channel with the target infidelity. We model initial state preparation and final measurement error as independent bit flip errors on each qubit, and we sample each qubit's error rate at random such that the average state preparation (measurement) error rate per qubit is 0.005 (0.01). Fig 4 shows the fidelity estimates from these simulations. For all error models, the estimated instrument fidelity is within 1σ of the true fidelity. We observe lower uncertainty in the estimates than observed in our simulations with larger n , which we expect due to eliminating uncertainty from sampling MCM-CB subexperiments (note, however, that the uncertainty also depends on the variance of the USI parameters, which is not fixed across our simulations).

B. Simulations of MCM-CB with Additional Error Models

The accuracy of the MCM-CB fidelity estimate depends on the properties of the USI error model. This is because (1) MCM-CB only samples a subset of MCM-CB subexperiments, hence learning only a subset of the USI parameters, and (2) MCM-CB uses a geometric mean to approximate the arithmetic mean of products of USI parameters. To explore this effect, we study the performance of MCM-CB with a different class of error models than in the simulations presented in the main text. We simulated MCM-CB with $n - m = 4, 6, 8$ unmeasured qubits and $m = 1, 2$ measurements in which we performed $K = 100$ MCM-CB subexperiments. We sampled USIs $\bar{M} = \mathcal{E}_{\text{post}}(\mathcal{T} \otimes \mathbb{I}_{n-m})\mathcal{L}\mathcal{E}_{\text{pre}}$ where \mathcal{E}_{pre} and $\mathcal{E}_{\text{post}}$ each have 100 random nonzero Pauli error rates, chosen so that the infidelity of \mathcal{E}_{pre} is $5p$ and the infidelity of $\mathcal{E}_{\text{post}}$ is p . \mathcal{T} consists of single-qubit depolarizing noise on each unmeasured qubit, with the infidelity of each qubit sampled from a normal distribution with mean p and standard deviation $0.2p$. We sample USIs for 120 uniformly-spaced values $p \in [0.0001, 0.0601]$. We model initial state preparation and final measurement error in the same way as in the simulations in the previous section. Fig 5 shows the fidelity estimates from these simulations. The MCM-CB estimate is within 2.5σ of the true fidelity for all error models.

The simulations presented so far all use a fixed average rate of state preparation and measurement (SPAM) error. To provide further evidence that our method is robust to SPAM error, we also simulated our method with varied-strength SPAM error. We show the results of these simulations in Fig. 5(b). We ran MCM-CB with independent bit flip error on each qubit immediately after state preparation and immediately prior to final measurement, and we varied the average per-qubit error rate p from 0 to 0.02. To generate the bit flip error rates, for both state preparation and measurement error, we sample uniform random error probabilities and normalize them so that their total is $pn/2$. We observe no systematic effect of the magnitude of the SPAM error on the accuracy of MCM-CB. However, higher SPAM error leads to increased uncertainty in the estimates.

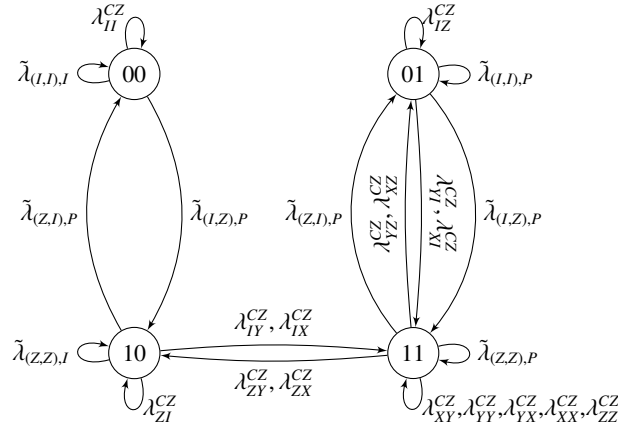


FIGURE 6. **MCM-CB of MCM+CZ.** Pattern transfer graph for a gate set consisting of single-qubit MCMs and a CZ gate. We label the edges with bit strings denoting the support of Pauli operators (e.g., 01 corresponds to the Pauli operators $IX, IY,$ and IZ). We use P to denote any non-identity single-qubit Pauli operator.

C. Investigating MCM-CB Subexperiment Sampling in Simulation

In Fig. 2 of the main text, we simulated MCM-CB with three error models. These models consist of a USI $\overline{\mathcal{M}} = \mathcal{E}_{\text{post}}(\mathcal{T} \otimes \mathbb{I}_{n-m})\mathcal{L}\mathcal{E}_{\text{pre}}$, and have the following forms:

1. (“Sparse”) \mathcal{T} , \mathcal{E}_{pre} , and $\mathcal{E}_{\text{post}}$ have each have 2^n nonzero Pauli errors, sampled in the same manner as the simulations presented in the main text, such that \mathcal{T} has infidelity 0.04 and each \mathcal{E}_{pre} , and $\mathcal{E}_{\text{post}}$ have infidelity 0.01.
2. (“Depolarizing+MCM error with crosstalk”) \mathcal{T} consists of single-qubit local depolarizing error, with each qubit’s error rate chosen from a normal distribution with mean 0.01 and standard deviation 0.002. Each \mathcal{E}_{pre} and $\mathcal{E}_{\text{post}}$ have of 2^n randomly sampled nonzero Pauli error rates. \mathcal{E}_{pre} and $\mathcal{E}_{\text{post}}$ are sampled to have the same fidelity (0.01).
3. (“Depolarizing+pre-MCM error with crosstalk”) \mathcal{T} consists of single-qubit local depolarizing error sampled from a normal distribution with mean 0.005 and standard deviation 0.0001, \mathcal{E}_{pre} consists of 2^n randomly-sampled Pauli errors, and $\mathcal{E}_{\text{post}} = \mathbb{I}_n$ with total infidelity 0.02.

III. LAYER SET CYCLE BENCHMARKING

In this section, we expand on the example of performing MCM-CB with a 2-qubit layer set consisting of two layers: a controlled Z (CZ) gate (between two qubits Q0 and Q1) and a single-qubit MCM (which we will assume is on Q0, but the case of an MCM on Q1 is analogous). To clarify the position of the MCM, we will use the notation $\tilde{\lambda}_{(Q_1, Q_2), P}$ to denote the PTM elements of the USI of the MCM layer. We model the CZ gate’s error as a post-gate stochastic Pauli channel with eigenvalues λ_Q^{CZ} and Pauli error rates p_Q for $Q \in \mathbb{P}_2$. The pattern transfer graph for this layer set is shown in Fig. III. The cycle space of this graph fully describes the learnable parameters of this layer set for MCM-CB with arbitrary single-qubit gates between layers, which are as follows.

- Learnable with MCM-only CB: $\tilde{\lambda}_{(Z,I),I}, \tilde{\lambda}_{(I,Z),I}, \tilde{\lambda}_{(I,I),P}$, and $\tilde{\lambda}_{(Z,Z),P}$, and $\tilde{\lambda}_{(Z,I),P}, \tilde{\lambda}_{(I,Z),P}$ for $P, P' = X, Y, Z$
- Learnable with CZ-only CB: $\lambda_{II}^{\text{CZ}}, \lambda_{IZ}^{\text{CZ}}, \lambda_{ZI}^{\text{CZ}}, \lambda_{XY}^{\text{CZ}}, \lambda_{YY}^{\text{CZ}}, \lambda_{YX}^{\text{CZ}}, \lambda_{XX}^{\text{CZ}}, \lambda_{ZZ}^{\text{CZ}}, \lambda_{IX}^{\text{CZ}}, \lambda_{ZX}^{\text{CZ}}, \lambda_{IY}^{\text{CZ}}, \lambda_{ZY}^{\text{CZ}}, \lambda_{IX}^{\text{CZ}}, \lambda_{ZY}^{\text{CZ}}, \lambda_{IY}^{\text{CZ}}, \lambda_{ZY}^{\text{CZ}}, \lambda_{XI}^{\text{CZ}}, \lambda_{XZ}^{\text{CZ}}, \lambda_{YI}^{\text{CZ}}, \lambda_{XZ}^{\text{CZ}}, \lambda_{XI}^{\text{CZ}}, \lambda_{YZ}^{\text{CZ}}$, and $\lambda_{YI}^{\text{CZ}}, \lambda_{YZ}^{\text{CZ}}$.
- Learnable with CZ+MCM CB: $\lambda_{ZY}^{\text{CZ}} \tilde{\lambda}_{P,(Z,I)}, \lambda_{IY}^{\text{CZ}} \tilde{\lambda}_{P,(I,Z)}, \lambda_{ZX}^{\text{CZ}} \tilde{\lambda}_{P,(Z,I)}, \lambda_{IX}^{\text{CZ}} \tilde{\lambda}_{P,(I,Z)}$ for $P = X, Y, Z$

Parameters learned by CB of a CZ and MCM sequence are *relational errors* that cannot be separated into CZ and MCM-only errors. As such, they can be difficult to interpret. Furthermore, we cannot perform a Walsh-Hadamard transform the relation errors into sums of Pauli error rates. As a step towards interpreting these error rates, we perform a first order expansion of these

parameters in the Pauli error rates. First, we express $\tilde{\lambda}_{(Z,I),P}$, $\tilde{\lambda}_{(I,Z),P}$ exactly in terms of Pauli error rates:

$$\tilde{\lambda}_{(Z,I),P} = \lambda_{0,0,P} - \lambda_{1,0,P} + \lambda_{0,1,P} - \lambda_{1,1,P} \quad (38)$$

$$= p_{0,0} - p_{1,0} + p_{0,1} - p_{1,1} - 2 \left(\sum_{P':[P,P'] \neq 0} p_{0,0,P'} - p_{1,0,P'} + p_{0,1,P'} - p_{1,1,P'} \right) \quad (39)$$

$$= 1 - 2(p_{0,1} + p_{1,1}) - 2 \left(\sum_{P':[P,P'] \neq 0} p_{0,0,P'} - p_{1,0,P'} + p_{0,1,P'} - p_{1,1,P'} \right), \quad (40)$$

where $p_{a,b}$ denotes the probability of pre-measurement MCM error $\mathcal{X}^{\otimes a}$ and post-measurement error $\mathcal{X}^{\otimes b}$, and $p_{a,b,P}$ denotes the probability of pre-measurement error $\mathcal{X}^{\otimes a}$, post-measurement error $\mathcal{X}^{\otimes b}$, and error P on the unmeasured qubits. Analogously,

$$\tilde{\lambda}_{(I,Z),P} = 1 - 2(p_{1,0} + p_{1,1}) - 2 \left(\sum_{P':[P,P'] \neq 0} p_{0,0,P'} + p_{1,0,P'} - p_{0,1,P'} - p_{1,1,P'} \right), \quad (41)$$

We now compute the CZ-MCM relational parameters and drop second order terms,

$$\lambda_{ZX}^{CZ} \tilde{\lambda}_{(Z,I),P} \approx 1 - 2(p_{XI} + p_{XX} + p_{YI} + p_{YX} + p_{ZY} + p_{ZZ} + p_{IY} + p_{IZ}) - 2(p_{1,0} + p_{1,1}) - 2 \left(\sum_{P':[P,P'] \neq 0} p_{0,0,P'} - p_{1,0,P'} + p_{0,1,P'} - p_{1,1,P'} \right) \quad (42)$$

$$= 1 - 2(p_{XI} + p_{XX} + p_{YI} + p_{YX} + p_{ZY} + p_{ZZ} + p_{IY} + p_{IZ}) - 2(p_{1,0,I} + p_{1,1,I} + p_{1,0,P} + p_{1,1,P}) - 2 \left(\sum_{P':[P,P'] \neq 0} p_{0,0,P'} + p_{0,1,P'} \right) \quad (43)$$

$$\lambda_{ZY}^{CZ} \tilde{\lambda}_{(Z,I),P} \approx 1 - 2(p_{XI} + p_{XY} + p_{YI} + p_{YY} + p_{ZX} + p_{ZZ} + p_{IX} + p_{IZ}) - 2(p_{1,0} + p_{1,1}) - 2 \left(\sum_{P':[P,P'] \neq 0} p_{0,0,P'} - p_{1,0,P'} + p_{0,1,P'} - p_{1,1,P'} \right) \quad (44)$$

$$= 1 - 2(p_{XI} + p_{XY} + p_{YI} + p_{YY} + p_{ZX} + p_{ZZ} + p_{IX} + p_{IZ}) - 2(p_{1,0,I} + p_{1,1,I} + p_{1,0,P} + p_{1,1,P}) - 2 \left(\sum_{P':[P,P'] \neq 0} p_{0,0,P'} + p_{0,1,P'} \right) \quad (45)$$

$$\lambda_{IX}^{CZ} \tilde{\lambda}_{(I,Z),P} \approx 1 - 2(p_{IY} + p_{IZ} + p_{XY} + p_{XZ} + p_{YY} + p_{YZ} + p_{ZY} + p_{ZZ}) - 2(p_{0,1} + p_{1,1}) - 2 \left(\sum_{P':[P,P'] \neq 0} p_{0,0,P'} + p_{1,0,P'} - p_{0,1,P'} - p_{1,1,P'} \right) \quad (46)$$

$$= 1 - 2(p_{IY} + p_{IZ} + p_{XY} + p_{XZ} + p_{YY} + p_{YZ} + p_{ZY} + p_{ZZ}) - 2(p_{0,1,I} + p_{1,1,I} + p_{0,1,P} + p_{1,1,P}) - 2 \left(\sum_{P':[P,P'] \neq 0} p_{0,0,P'} + p_{1,0,P'} \right) \quad (47)$$

$$\lambda_{IY}^{CZ} \tilde{\lambda}_{(I,Z),P} \approx 1 - 2(p_{IX} + p_{IZ} + p_{XX} + p_{XZ} + p_{YX} + p_{YZ} + p_{ZX} + p_{ZZ}) - 2(p_{0,1} + p_{1,1}) - 2 \left(\sum_{P':[P,P'] \neq 0} p_{0,0,P'} + p_{1,0,P'} - p_{0,1,P'} - p_{1,1,P'} \right) \quad (48)$$

$$= 1 - 2(p_{IX} + p_{IZ} + p_{XX} + p_{XZ} + p_{YX} + p_{YZ} + p_{ZX} + p_{ZZ}) - 2(p_{0,1,I} + p_{1,1,I} + p_{0,1,P} + p_{1,1,P}) - 2 \left(\sum_{P':[P,P'] \neq 0} p_{0,0,P'} + p_{1,0,P'} \right) \quad (49)$$

We see that by performing CB with the CZ+MCM germ, we do not learn $p_{0,1,P'}$ $p_{1,0,P'}$ in isolation, but we learn information about $p_{0,1,P'} - p_{1,0,P'}$ in combination with many CZ error rates.

It is also useful to expand the parameters learned by MCM-CB of the MCM layer to first order. This offers an alternate approach to estimating Pauli error probabilities using MCM-CB data, instead of the approximation $\tilde{\lambda}_{(I,Z),P_{\text{rest}}} \approx \tilde{\lambda}_{(Z,I),P_{\text{rest}}} \approx$

$\hat{p}_{(I,Z),P_{\text{rest}}}$ used in the main text. To first order, the parameters we learn in product are

$$\tilde{\lambda}_{(Z,I),P}\tilde{\lambda}_{(I,Z),P} = 1 - 2(p_{0,1} + p_{1,0} + 2p_{1,1}) - 4 \left(\sum_{P':\{P,P'\} \neq 0} p_{0,0,P'} - p_{1,1,P'} \right) \quad (50)$$

$$\tilde{\lambda}_{(Z,I),I}\tilde{\lambda}_{(I,Z),I} = 1 - 2(p_{0,1} + p_{1,0} + 2p_{1,1}). \quad (51)$$

The second equation allows us to learn $p_{1,1}$ and $p_{0,0}$, because we can learn $p_{0,1} + p_{1,0}$ from $\tilde{\lambda}_{(I,I),I}$ and $\tilde{\lambda}_{(Z,Z),I}$. Furthermore, to first order,

$$\tilde{\lambda}_{(Z,I),I}\tilde{\lambda}_{(I,Z),I} - \tilde{\lambda}_{(Z,I),P}\tilde{\lambda}_{(I,Z),P} = 4 \left(\sum_{P':\{P,P'\} \neq 0} p_{0,0,P'} - p_{1,1,P'} \right) \quad (52)$$

Using the above equation, we can estimate $p_{0,0,P}$, $p_{1,1,P}$ and $p_{0,1,P} + p_{1,0,P}$ for $P = X, Y, Z$ using $\tilde{\lambda}_{(Z,I),I}\tilde{\lambda}_{(I,Z),I}$ and all $\tilde{\lambda}_{(Z,I),P}\tilde{\lambda}_{(I,Z),P}$, $\tilde{\lambda}_{(Z,Z),P}$ and $\tilde{\lambda}_{(I,I),P}$.

IV. DETAILS OF IBM Q DEMONSTRATIONS

In this section, we provide additional details of our demonstrations of MCM-CB on IBM Q processors. Figure 7(a) shows the MCM-CB decay parameters $\hat{p}_{P_{\text{meas}},(P_{\text{rest}},Q)}$ from our 4-qubit MCM-CB demonstration on `ibm_osaka`. We omit the decay parameters $\hat{p}_{P_{\text{meas}},(I,Z)}$ because $p_{P_{\text{meas}},(I,Z)} = p_{P_{\text{meas}},(Z,I)}$, and our estimates of $p_{P_{\text{meas}},I,Z}$ and $p_{P_{\text{meas}},(I,Z)}$ were approximately equal. We estimated the eigenvalues of the $\mathcal{T}_{a,b}$ using

$$\hat{\lambda}_{0,0,P} = \frac{1}{4}(\hat{p}_{P,(I,I)} + \hat{p}_{P,(Z,Z)} + 2\hat{p}_{P,(Z,I)}) \quad (53)$$

$$\hat{\lambda}_{0,1,P} + \hat{\lambda}_{1,0,P} = \frac{1}{2}(\hat{p}_{P,(I,I)} - \hat{p}_{P,(Z,Z)}) \quad (54)$$

$$\hat{\lambda}_{1,1,P} = \frac{1}{4}(\hat{p}_{P,(I,I)} + \hat{p}_{P,(Z,Z)} - 2\hat{p}_{P,(Z,I)}). \quad (55)$$

Note that our estimates for $\lambda_{0,0,P}$, $\lambda_{1,1,P}$ use the approximation $\tilde{\lambda}_{P_{\text{rest}},(I,Z)} \approx \tilde{\lambda}_{P_{\text{rest}},(Z,I)} \approx p_{P_{\text{rest}},(Z,I)}$ for all P_{rest} . We then perform a Walsh-Hadamard transform on each of the sets of values $\{\hat{\lambda}_{0,0,P}\}$, $\{\hat{\lambda}_{1,1,P}\}$, and $\{\hat{\lambda}_{0,1,P} + \hat{\lambda}_{1,0,P}\}$ to estimate the Pauli error rates of the MCM layer [14]. Figure 7(b) shows all estimated Pauli error rates. Table I shows the calibration data for `ibm_osaka` from the time we ran our MCM-CB circuits.

In addition to our 4-qubit demonstration, we ran 2-qubit MCM-CB of a layer consisting of an MCM (on Q13) and an idling qubit (Q14) of `ibm_torino`. Figure 7(c) shows all MCM-CB decay parameters from this demonstration, and Fig. 7(d) shows all estimated Pauli error rates for the MCM layer, using the same approach as in our 4-qubit MCM-CB demonstration to perform the estimation. For this layer, single MCM bit flip errors are the dominant source of error [0.009(1)], followed by Y, X, and Z errors on the unmeasured qubit. The calibration data from the time of execution is shown in Table II.

qubit	T_1 (us)	T_2 (us)	frequency (GHz)	anharmonicity (GHz)	readout error	Pr(prepare 1, measure 0)	Pr(prepare 0, measure 1)	readout length (ns)
Q40	214.84	7.93	4.89	-0.31	0.006	0.006	0.007	1400.00
Q41	188.37	101.57	4.99	-0.31	0.040	0.044	0.036	1400.00
Q42	226.91	5.93	4.79	-0.31	0.010	0.012	0.007	1400.00
Q43	409.52	135.55	4.93	-0.31	0.018	0.006	0.030	1400.00

TABLE I. **IBM Q Calibration data for `ibm_osaka`.** Calibration data from the time of our 4-qubit MCM-CB demonstration.

qubit	T_1 (us)	T_2 (us)	frequency (GHz)	anharmonicity (GHz)	readout error	Pr(prepare 1, measure 0)	Pr(prepare 0, measure 1)	readout length (ns)
Q13	288.34	93.44	4.73	0.00	0.008	0.012	0.003	1400.00
Q14	129.27	29.80	4.74	-0.31	0.085	0.091	0.079	1400.00

TABLE II. **IBM Q Calibration data for `ibm_torino`.** Calibration data from the time of our 2-qubit MCM-CB demonstration.

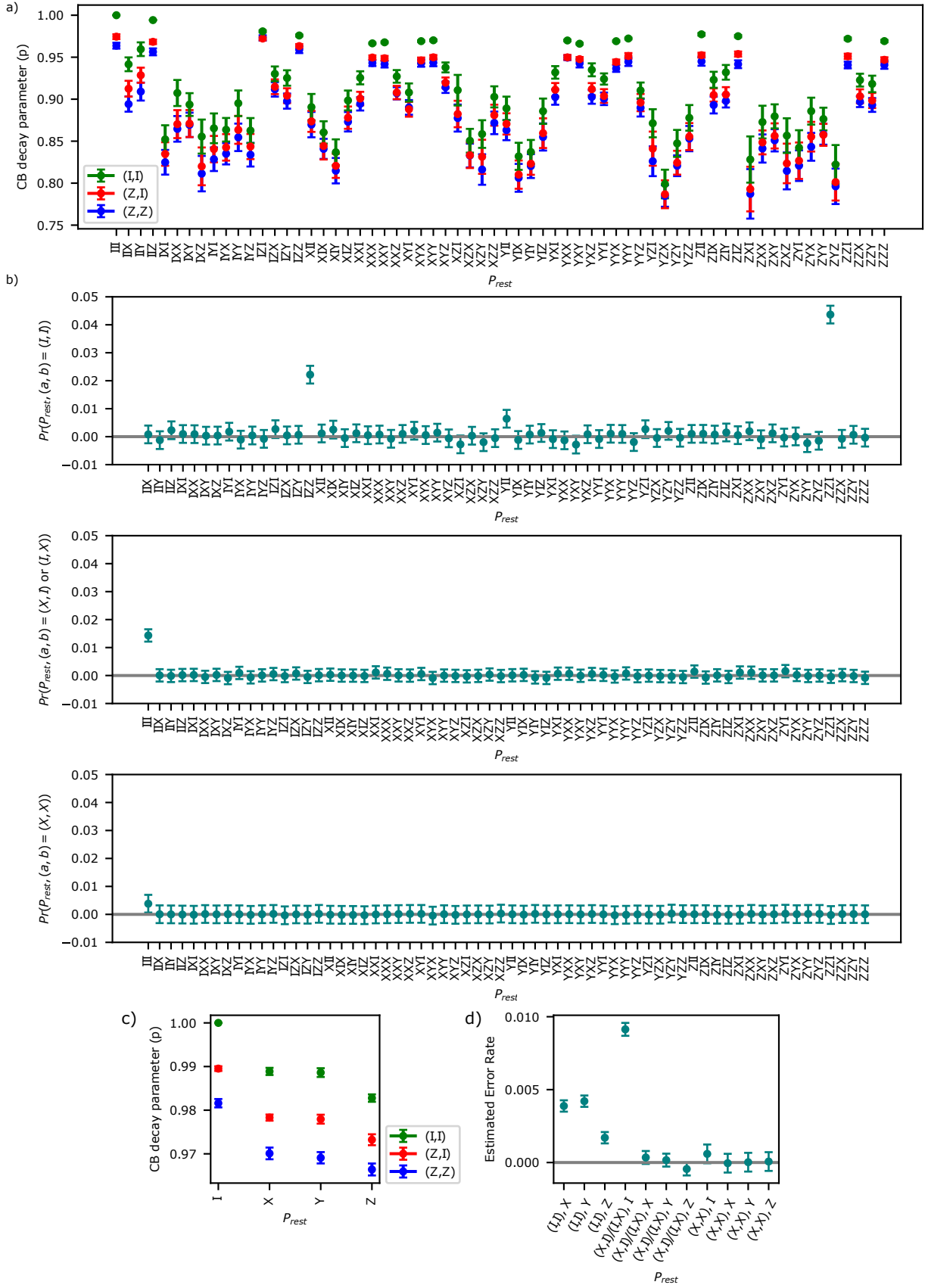


FIGURE 7. **MCM-CB on IBM Q.** (a) All extracted MCM-CB parameters $P_{P_{rest},(P_{meas},Q)}$ from our demonstration of MCM-CB of a 4-qubit layer with one MCM on `ibm_osaka`. (b) The estimated Pauli error rates, which we obtain by performing a Walsh-Hadamard transformation on subsets of the MCM-CB decay parameters with fixed (P_{meas}, Q) and using the approximation $\tilde{\lambda}_{P_{rest},(P_{meas},Q)}$ for $P_{meas} \neq Q$. (c) All extracted parameters from 2-qubit CB MCM-CB of a single-qubit MCM on `ibm_torino`. The estimated fidelity of the MCM layer is 0.980(1). (d) Estimated Pauli error rates for the 2-qubit MCM layer.